A diagnostic study of the Arctic Ocean winter density-driven circulation in 1973–79

IGOR V. POLYAKOV and NIKOLAY Yu. DORONIN

Polyakov, I. V. & Doronin, N. Yu. 1999: A diagnostic study of the Arctic Ocean winter density-driven circulation in 1973–79. *Polar Research 18(1)*, 27–38.

Diagnostic computations of density-driven circulation for seven winters from 1973 through 1979 were carried out. The only forcing was provided by observed temperature and salinity data collected during on-site Russian winter surveys in 1973–79. Computed circulations from 1973 through 1978 were close to the mean circulation obtained earlier by averaging observed 1973–79 temperature and salinity (Polyakov & Timokhov 1994). The computed 1979 density-driven circulation flowed counter-clockwise to the north of the Laptev Sea. This circulation pattern was caused by an anomalous salinity distribution associated with changes in the atmospheric circulation regime in 1979. Prevailing offshore winds blew fresh water from the Laptev and East Siberian shelves toward Fram Strait. Fresh water was exchanged for saltier intermediate water that upwelled to the surface along the slope. The observed surface salinity anomalies at the continental slope of the Laptev Sea in 1979 increased by several salinity units. One may speculate that the same process may have caused the observed salinification of the Eurasian Basin in the 1990s.

I. V. Polyakov, International Arctic Research Center, University of Alaska Fairbanks, Fairbanks, AK, 99775-7221, USA; N. Yu. Doronin, EcoShelf, P.O. Box 880, 199048, St. Petersburg, Russia.

Introduction

The characteristics of surface currents in the Arctic Ocean are well known owing to a number of observations obtained from drifting buoys (Fig. 1; Thorndike & Colony 1982), and from manned ice drift camp trajectories (Treshnikov 1985). The major features of the circulation are the Trans Polar Drift Stream, which flows from the Chukchi Sea slope toward Fram Strait, and the anticyclonic Beaufort Gyre. However, analysing atmospheric pressure charts and drift patterns of manned polar stations, Gudkovich (1961) pointed out that summer ice drift and surface water circulation may alternate between anticyclonic and cyclonic. Serreze et al. (1989) used drifting buoy data for 1979–85 to demonstrate that in late summer to early autumn the ice motion can indeed become cyclonic. Using modelling results and observational data, Proshutinsky & Johnson (1997) have found that in the central Arctic, wind circulation and resulting wind-driven motion in the upper ocean alternate between anticyclonic and cyclonic. Shifts between these two regimes occur at 5 to 7 year intervals, resulting in a 10 to 15 year period. The anticyclonic circulation regime has been observed for 1946–52, 1958–62, 1972–79, and 1984–88. The cyclonic circulation regime prevailed during 1953–57, 1963–71, 1980–83, and 1989–96.

Measurements of the deep ocean circulation are difficult due to year-round ice cover. Aagaard (1989) summarized existing observations on deep currents and concluded that general water transport in the Polar Basin takes the form of narrow boundary currents along the ocean peripheries. These currents move opposite to surface currents.

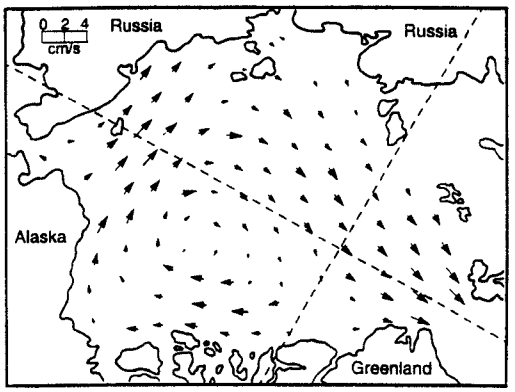

Fig. 1. Surface currents in the Arctic Ocean (adapted from Thorndike & Colony 1982, *J. Geophys. Res. 87 [C8]*, p. 5850; copyright by the American Geophysical Union; printed with permission of the authors and AGU).

In the interior of the Canadian Basin the currents are weak, and their kinetic energy is concentrated in mesoscale eddies. According to Aagaard, thermohaline currents are the main component of Arctic Ocean subsurface circulation, and their intensity is comparable to that of the thermohaline currents in the Greenland Sea.

Modelling studies help to compensate for the lack of observational information and to improve understanding of the mechanisms affecting natural processes. Häkkinen (1993) used a coupled ice-ocean model to examine ice and ocean behaviour for an explanation of the salinity anomaly in the Greenland Sea during the 1960s. She demonstrated the important role of wind-driven circulation in the Arctic in the formation of temperature and salinity anomalies in the North Atlantic. Zhang et al. (1998) found a strong link between the wind pattern over the central Arctic and the Atlantic water transport from the Greenland and Barents Seas into the Arctic Ocean, and pointed out that in the 1990s an increased penetration of the Atlantic water from the Barents Sea caused salinization and warming in the Eurasian Basin. Previously, Steele & Boyd (1998) had used observational data to reveal a remarkable salinification and warming there. They stressed that the salinity anomaly in the upper ocean layer reached up to several parts per thousand (ppt). According to Steele & Boyd (1998), this anomalous salinization had not been observed before.

In this study we use Russian observational data to demonstrate that observed salinization of the upper ocean in the 1990s is not unique, and that analogous event occurred in 1979. Using simple diagnostic calculations we show how ocean thermohaline circulation responds to this salinity anomaly.

Given the forcing, the diagnostic method renders a three-dimensional distribution of current for the steady-state flow. The first diagnostic calculation using an integrated vorticity balance equation for the stream function appeared in 1969 (Sarkisyan 1969). Holland & Hirschman (1972) produced a steady-state solution for the North Atlantic circulation using a primitive equation model. Sarmiento & Bryan (1982) used a robust model with a Newtonian damping factor to force the temperature and salinity toward climatological values. This methodology was widely used later; for example, it was applied by Hibler & Bryan (1987) and Zhang et al. (1998) in their coupled sea ice-ocean models for the Arctic.

Table 1. Number of oceanographic stations for each winter survey in 1973–79.

Year	1973	1974	1975	1976	1977	1978	1979
Number of stations	172	166	182	152	117	127	118

Temperature and salinity data

In this study, we used temperature and salinity data for each winter from 1973 through 1979, with measurements covering most of the Arctic Ocean. The number of oceanographic stations for each year is presented in Table 1. The areas covered by the observations varied. The largest areas were measured in 1974–76. The number of stations in 1973 was approximately the same as in 1974–76, but did not include a region adjacent to the Canadian Archipelago. Temperature and salinity data for the Arctic marginal seas in 1977 were not available, and we used data for the central Arctic only. Observations in 1978 and 1979 also omitted an area adjacent to the Canadian Archipelago. The positions of the oceanographic stations in 1979 are shown in Fig. 2. Despite the lower number of oceanographic stations in 1977–79, the data density was approximately the same as in 1974–76 due to some reduction of the total area of observations.

Aircraft were used for all surveys. The planes landed on the drift ice, holes were drilled, the water temperature was measured, and water samples were taken using Nansen bottles. Salinity was determined by silver chloride titration. The precision of the temperature and salinity measurements was to 0.01°C and 0.01 ppt, respectively. The measurements were carried out at Russian standard oceanographic depths of 5, 10, 15, 20, 25, 30, 40, 50, 75, 100, 150, 200, 250, 300, 400, 500, 600, 750 and 1000 m, and at 500 m intervals from 1000 m to the bottom. The data were examined to correct obvious errors; missing values in the vertical profiles were estimated by linear interpolation from neighbouring points; and spline-interpolation was used to calculate the temperature and salinity values at every grid point.

Model and design of numerical experiments

A three-dimensional primitive equation z-coordinate free surface ocean model was used in this

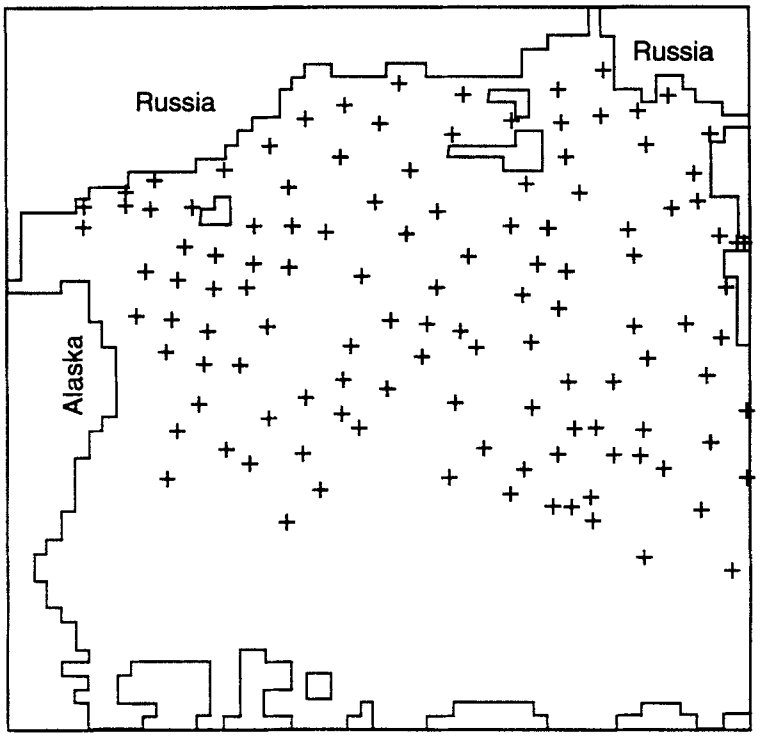

Fig. 2. Positions of stations during Russian oceanographic survey in 1979.

study. As a part of a coupled ice-ocean model, it has been applied, for example, to simulate currents and sea level elevations in the Arctic Ocean (Polyakov et al. 1998). The model incorporates a turbulent closure model, which follows from the equation for turbulent kinetic energy and is a relation between the eddy viscosity coefficient, vertical shear of the horizontal velocity, and buoyancy. A kinematic boundary condition for the vertical velocity at the surface allows reproduction of fast external surface gravity waves, including tides. The model incorporates splitting of the original three-dimensional momentum equations for the depth-averaged equations and for the vertically varying equations (Blumberg & Mellor 1983; Song & Haidvogel 1994). The horizontal viscosity coefficient is constant and equal to $5 \cdot 10^6$ cm^2/s. The finite-difference approximation used in the model is described in Polyakov (1996). The numerical model domain incorporates uniform horizontal resolution with an increment of $\Delta x = 55.56$ km (Fig. 3).

The diagnostic computation technique developed by Sarkisyan (1991) was used in these experiments. Given the density forcing, this diagnostic method renders a three-dimensional distribution of current for the steady-state flow. In this particular experiment, the only forcing was the density distribution for seven years starting with 1973 and ending with 1979. We applied the primitive equation ocean model, but the heat and salt balance equations were omitted because the density was assumed to be constant across time. At the open boundaries, zero sea level and zero velocity derivatives normal to the open boundary were specified. The position of the open boundary in every experiment was determined by available information on temperature and salinity. The locations of the oceanographic stations and the areas of the ocean covered by the observations varied from year to year. Sarkisyan (1991) showed that the effect of boundaries in diagnostic experiments may be traced in the grid points nearest to the boundaries only. Our results demonstrate the accuracy of this conclusion because there is no numerical noise in the computed velocities and sea level elevations at the open boundaries. Therefore, we did not apply any special method, such as the flow relaxation scheme (Engedahl 1995), to determine the velocity at the open boundary.

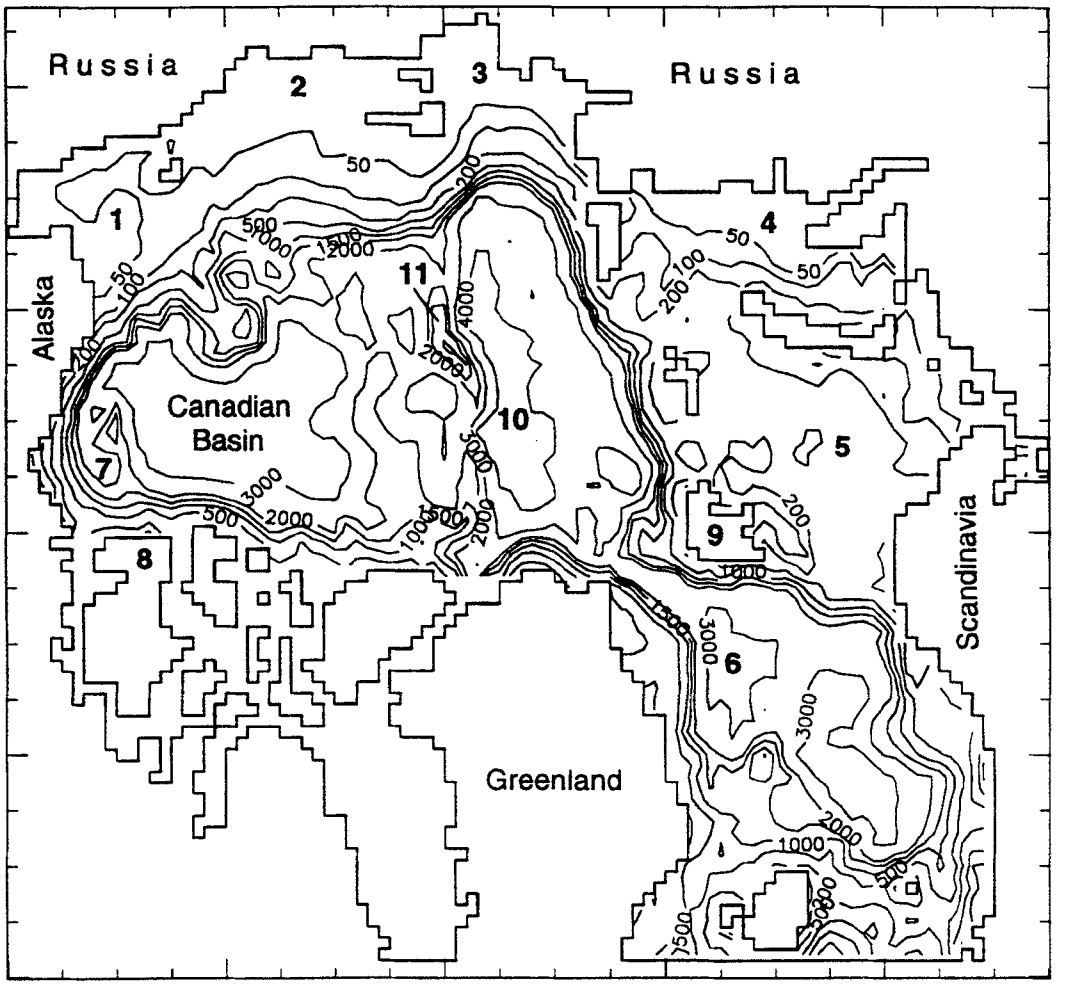

Fig. 3. The Arctic Ocean bathymetry. 1 = Chukchi Sea, 2 = East Siberian Sea, 3 = Laptev Sea, 4 = Kara Sea, 5 = Barents Sea, 6 = Greenland Sea, 7 = Beaufort Sea, 8 = Canadian Archipelago, 9 = Spitsbergen, 10 = Nansen Basin, 11 = Lomonosov Ridge.

There were seven diagnostic computations for each winter from 1973 through 1979. The time-dependent behaviour of volume-averaged mean total energy was used as a criterion of the steady-state solution. The time required to obtain a stable solution for each experiment varied from 22 to 30 days.

The ocean model was not coupled with an ice model in this study. The results of diagnostic computations of the density-driven circulation omitting the effects of wind seem relatively unaffected by the stresses between the drifting ice and the surface ocean currents. Moreover, Sarkisyan (1991) has argued that the oceanic density structure is adjusted to the wind forcing; therefore, the effect of winds is partly incorporated into the density field.

Results

The density-driven component of the Arctic Ocean circulation, computed by mean winter temperature and salinity for 1973–79, has been discussed in Polyakov & Timokhov (1994) and is presented in Fig. 4. The major features of the surface circulation are the Trans Polar Drift Stream and the anticyclonic Beaufort Gyre, with its corresponding positive sea level elevations of up to 30 cm in the

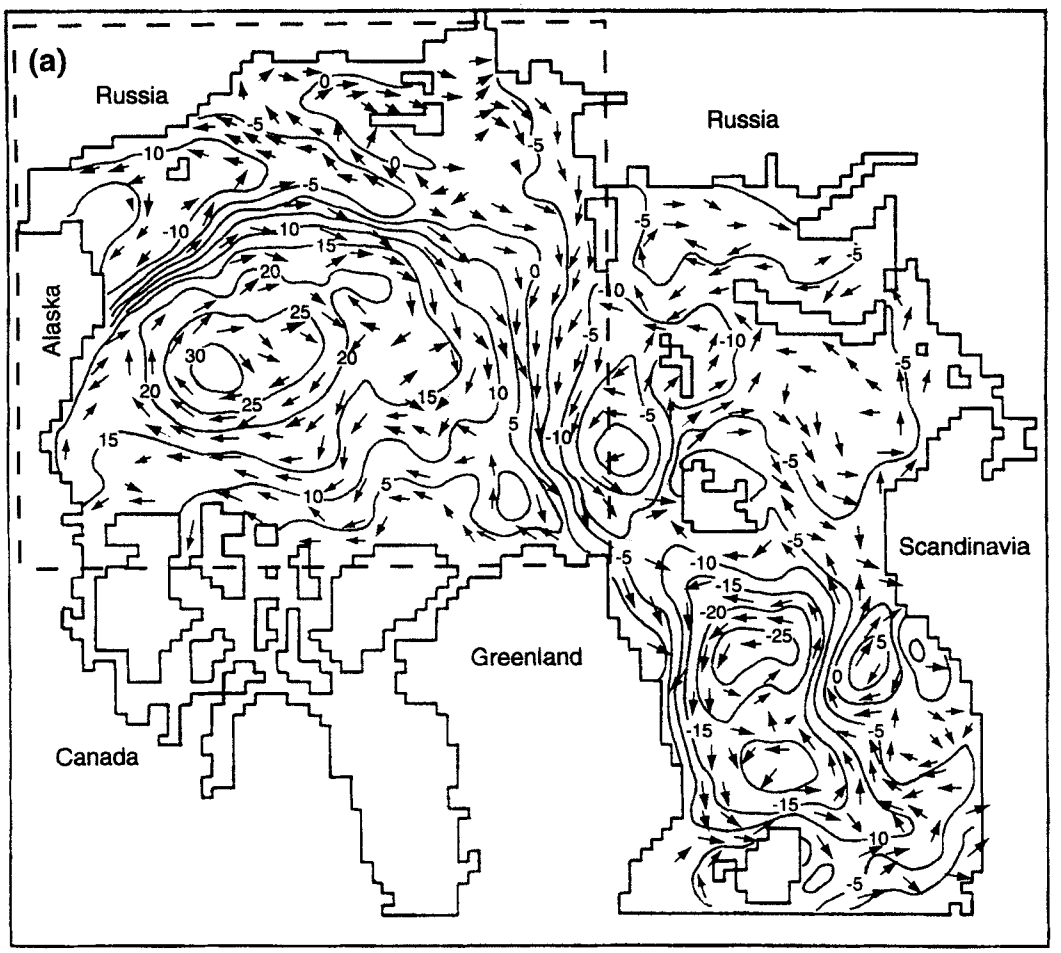

Fig. 4. Computed mean winter density-driven circulation in the Arctic Ocean. Dashed line delineates the area shown in Figs. 5–7. (a) Sea level elevation (cm) and surface currents. Vectors are plotted at every other grid point. (b) Near-bottom currents. Vectors are plotted at every grid point. Vectors with value less than 0.25 cm/s are not shown. The scale of vectors: arrow length of 0.5 d corresponds to current velocity $0.25 < V < 0.5$ cm/s; arrow length of 1 d corresponds to $0.5 < V < 2.5$ cm/s; arrow length of 1.5 d corresponds to $2.5 < V < 5.0$ cm/s; arrow length of 2 d corresponds to $5.0 < V < 10.0$ cm/s; and arrow length of 2.5 d corresponds to $V > 10.0$ cm/s. V is velocity magnitude, d is grid cell length. Area without observations has no vectors.

centre of the rotation. In the computed surface density-driven circulation, an anticyclonic gyre is generated by the salinity minimum at 250 m and deeper, located north and north-west of Greenland with relatively weak (up to 2–3 cm/s) currents; the corresponding sea level maximum is about 12 cm there. On the East Siberian Sea shelf, the westward coastal current obtained in our experiments contradicts the commonly accepted circulation pattern on this shelf (Gorshkov 1980). Nikiforov & Shpaikher (1980) depicted an eastward current there, but we do not know whether their circulation pattern was obtained by observations or by modelling. Note also that our computation omits the effect of winds, which is the major contributor to shallow water circulation. A complex balance of various forces that maintain the observed circulation on the Arctic shelves may be responsible for these different directions in the coastal currents. The computed currents maintain their direction with depth on the Siberian shelf and at the continental slope of the Chukchi and East Siberian seas. At the slope of the Laptev Sea the surface and near-bottom currents move in opposite directions. More typically, surface and bottom currents in the Arctic Ocean are directed at some angle to each

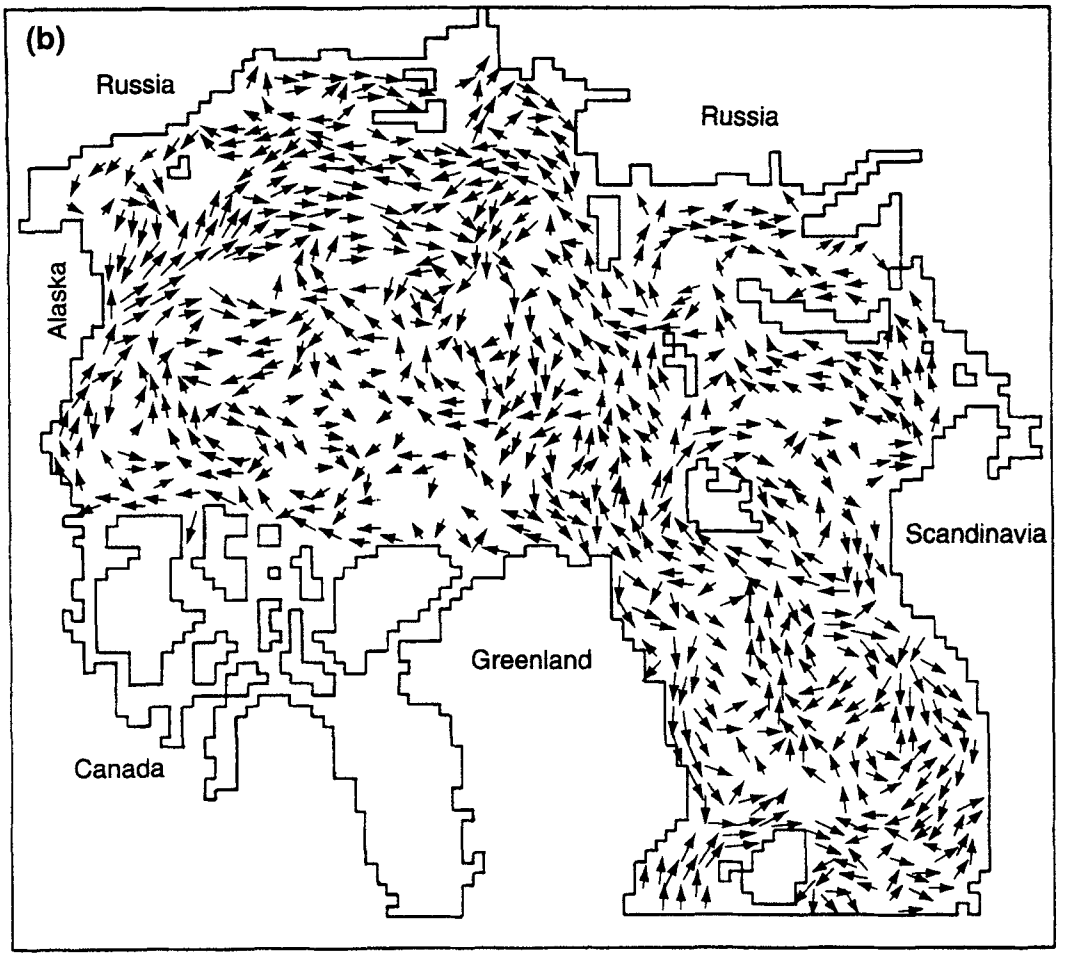

Fig. 4. Continued.

other, and the greater the velocity, the smaller the angle. This result contradicts Aagaard's suggestion (1989) that surface and deep circulations have opposite directions in the Arctic Ocean. Again, our computation does not take winds into account; wind-induced surface circulation may differ substantially from the density-driven circulation.

The sea level elevation and surface currents computed with the use of the winter density distributions for 1973, 1978 and 1979 are depicted in Figs. 5a, 6a and 7a. Figs. 5b, 6b and 7b show the corresponding near-bottom circulation. The computed density driven circulation during these years was in one way or another anomalous. The plots for 1974–77 are not presented because the computed circulation for these years was close to the mean circulation depicted in Fig. 4.

The variation in the location of the centre of anticyclonic rotation in the Beaufort Sea, determined by the local sea level maximum, is relatively small from 1973 to 1978. The part of the Trans Polar Drift Stream contiguous with the continental slope of the Arctic seas is stable, and is determined by the bottom topography. Away from the continental slope, the location of the Trans Polar Drift Stream becomes unstable from year to year with deviations up to 250–300 km. The thermohaline circulations on the shelves of the Chukchi, Laptev and East Siberian Seas have small temporal variations. Both the location and intensity of the anticyclonic gyre to the north and north-west of Greenland are variable in time. As a result, the sea level maximum in the averaged pattern is submerged and currents are weak (Fig.

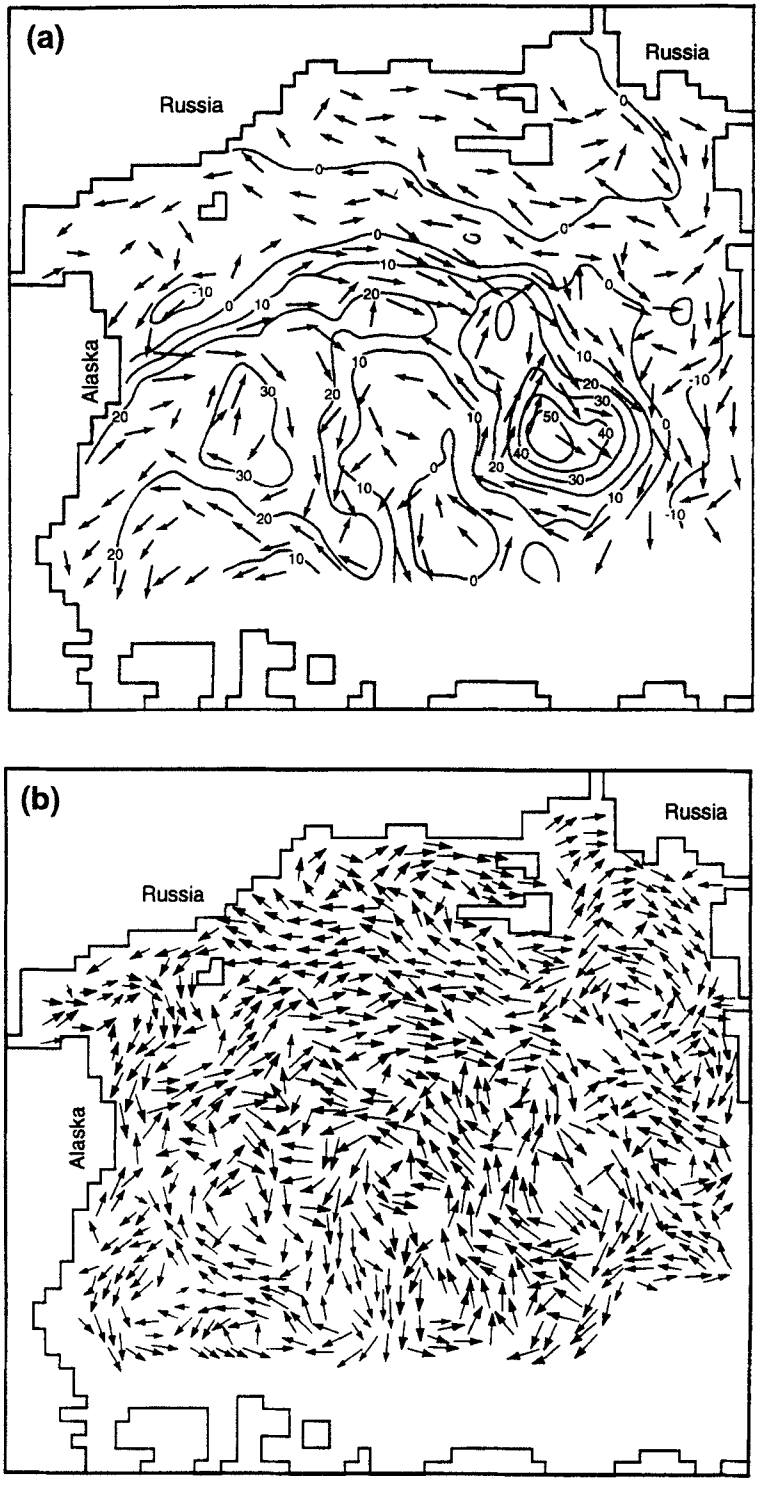

Fig. 5. Computed winter density-driven circulation in the Arctic Ocean in 1973. (a) Sea level elevation (cm) and surface currents. Vectors are plotted at every other grid point. (b) Near-bottom currents. Vectors are plotted at every grid point. Vectors with value less than 0.25 cm/s are not shown. Scale of vectors is shown in Fig. 4.

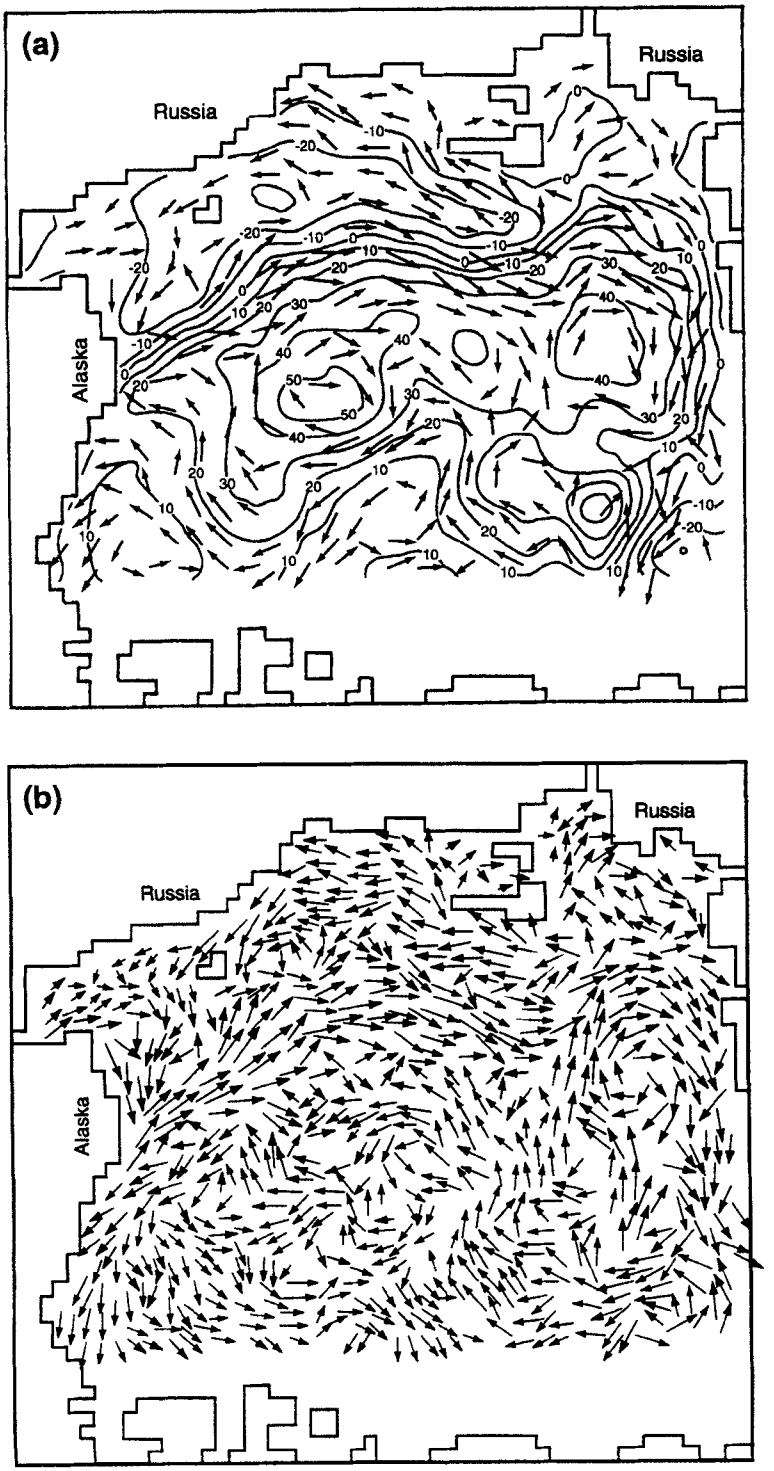

Fig. 6. Computed winter density-driven circulation in the Arctic Ocean in 1978. (a) Sea level elevation (cm) and surface currents. Vectors are plotted at every other grid point. (b) Near-bottom currents. Vectors are plotted at every grid point. Vectors with value less than 0.25 cm/s are not shown. Scale of vectors is shown in Fig. 4.

Table 2. The averaged kinetic energy of the winter thermohaline currents for 1973–79 (KJ).

Year	1973	1974	1975	1976	1977	1978	1979
Energy	0.28	0.11	0.09	0.05	0.08	0.41	0.21

4a). The intensity of the thermohaline circulation in 1973–78 was very different. Dynamic processes were especially pronounced in 1978 (Fig. 6), when the sea level elevation in the Beaufort Sea was greater than 50 cm, with a corresponding increase in the current velocity. Table 2 shows the averaged-over-the-domain kinetic energy of the density-driven currents. This characteristic confirms that density-driven circulation was particularly strong in 1978. At the same time, atmospheric processes during the winter of 1978 were very stable, with the extreme development of the Arctic high (Petrov 1983), which apparently resulted in increased water and ice circulation. The general water mass transport in deep layers is concentrated in relatively narrow currents along the continental slopes and ridges. In the abyssal areas the currents are weak and form topographic eddies.

This conclusion does not seem to follow from plots presented; however, this apparent disagreement resides in the problem of plotting the vectors. Normalized vector plots, with vector length plotted as a percentage of the maximum vector length, would have shown only 3–4 narrow flows along the continental slope of Siberia, the Beaufort Sea, Spitsbergen, and along Lomonosov Ridge. The other vectors would have been reduced to points. Such plots would show the general mass transport and would agree well with Aagaard's conclusion (1989) that the maximum currents are at the Arctic Ocean margins. However, since this method would provide little information on the basin as a whole, we scaled the vectors, and each range is shown as a vector of a certain length. For example, an arrow length of 2.5 d (d is the length of the grid cell side) corresponds with all vectors with modules higher than 10 cm/s.

The computed density-driven circulation of 1979 is atypical (Fig. 7). The Trans Polar Drift Stream, and circulation in the Nansen Basin and on the shelf of the Chukchi and East Siberian seas are the opposite of average conditions (Fig. 4). But because the oceanographic survey in 1979 was carried out over a limited area of the Arctic Ocean it is not possible to draw a conclusion about the circulation in the Arctic Ocean as a whole.

Discussion

Diagnostic computations are a popular and inexpensive method of estimating circulation with the use of observational data and a mathematical model. However, such computations have at least two serious shortcomings: The first is the sensitivity of the solution to "noise" caused by non-stationary processes affecting the temperature and salinity fields. The second shortcoming is that the model topography disagrees with the observed temperature and salinity used in the computations. An adjustment method that has been suggested to reduce these weaknesses of the diagnostic approach (Sarkisyan & Demin 1983; Demin et al. 1991) consists of using diagnostic calculations that keep temperature and salinity constant in time, followed by a short-term prognostic computation. This method has been applied by Ezer & Mellor (1994) to simulate North Atlantic circulation. These authors note that their model yields dynamically adjusted velocities and sea level heights. We did not use any special method for the diagnostic computations because the level of numerical noise in the computed velocities and sea level elevations was relatively low.

The computed Trans Polar Drift Stream, the anticyclonic Beaufort Gyre, and currents over the shelf of the Arctic seas are the consistent elements of the Arctic thermohaline circulation from 1973 through 1978. A sea level elevation maximum with corresponding anticyclonic rotation to the north and north-west of Greenland is also persistent in the computed current patterns for 1973–78. However, large variability in this circulation resulted in a weak overall average. The general water mass transport in deep layers is concentrated in relatively narrow currents along the continental slopes and ridges. In the abyssal areas the currents are weak and form topographic eddies.

The computed density-driven circulation in 1979 was atypical when the direction of the major circulation branches was opposite to the mean pattern. The reason for this unusual situation lies with the anomalous salinity distribution in 1979. That was a transitional year between the anticyclonic (the 1970s) and cyclonic (the 1980s) circulation regimes (Proshutinsky & Johnson 1997), which implies that very different wind conditions existed in 1973–78 compared with 1979. A possible explanation of the anomalous salinity distribution in the Eurasian Basin in 1979

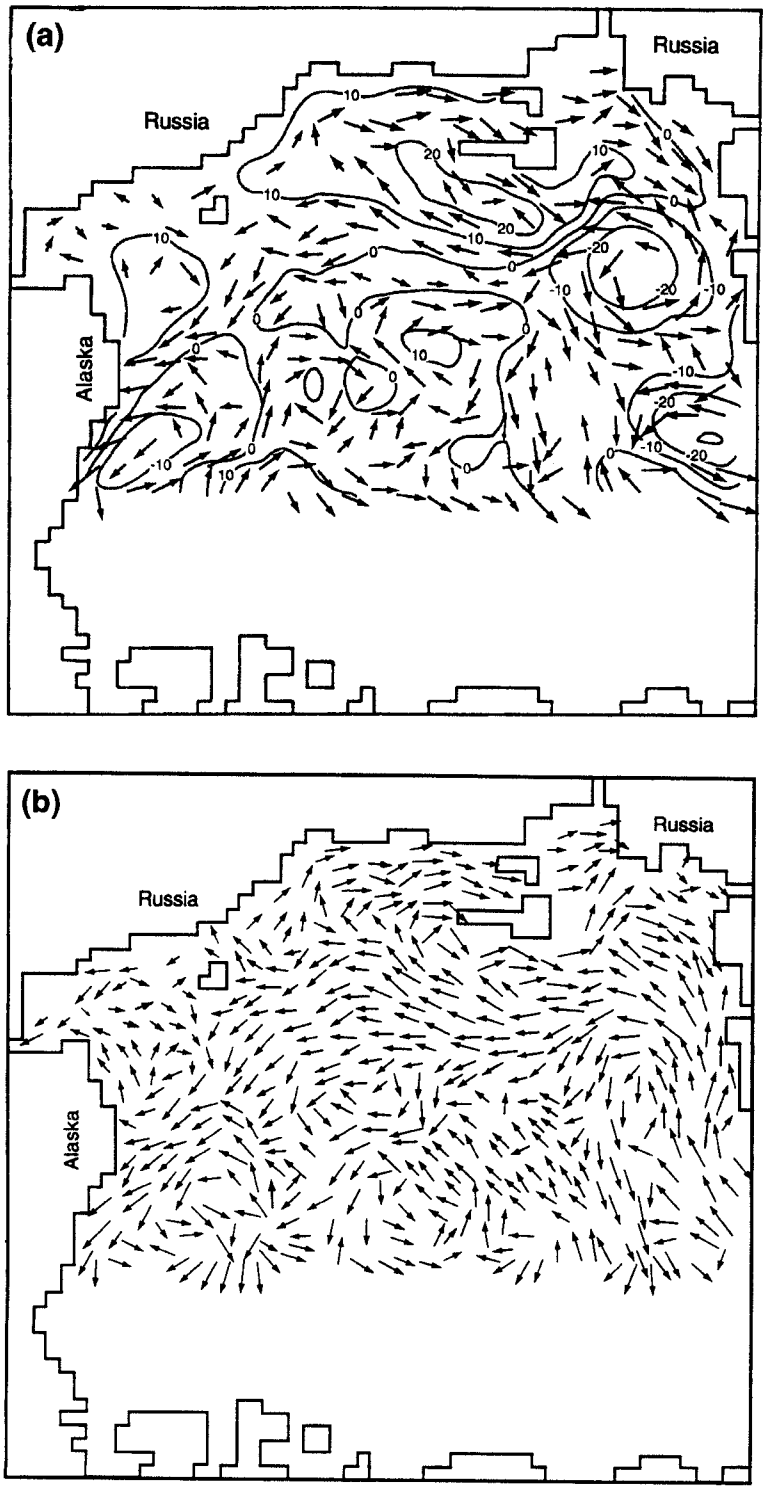

Fig. 7. Computed winter density-driven circulation in the Arctic Ocean in 1979. (a) Sea level elevation (cm) and surface currents. Vectors are plotted at every other grid point. (b) Near-bottom currents. Vectors are plotted at every grid point. Vectors with value less than 0.25 cm/s are not shown. Scale of vectors is shown in Fig. 4.

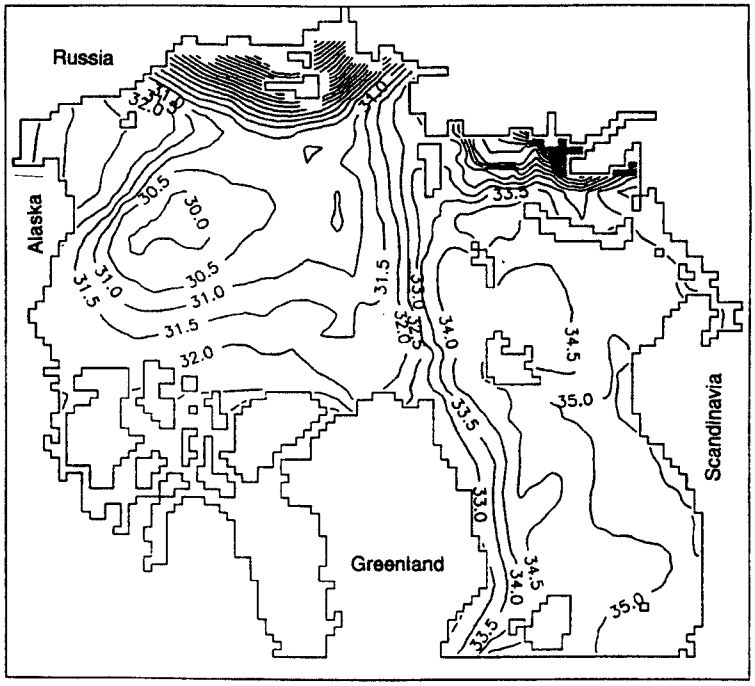

Fig. 8. Winter surface salinity (ppt) averaged over the period 1973–79. Contour interval is 0.5 ppt.

may be found in Nikiforov & Shpaikher (1980). They indicated that salinification and freshening of the upper ocean layer in this region of the Arctic is closely related to the atmospheric circulation, and suggested a scenario in which years with reduced atmospheric surface pressure had prevailing offshore winds that blew fresh surface water formed by Siberian river discharge and ice melt into the northern Laptev Sea. This surface water is replaced by the saltier underlying water of the Nansen Basin. The positive salinity anomalies to the north of the Laptev Sea, which were indicated by Russian observations, increased by up to several ppt.

Nikiforov & Shpaikher's (1980) scenario is confirmed by observational data from the Russian oceanographic surveys made in 1973–79. During 1973 through 1978, the surface salinity distribution was close to the mean, with a gradual decrease in salinity from the Siberian coast toward Greenland and a salinity minimum in the Beaufort Sea (Fig. 8). In 1979, the surface salinity was at a minimum in the central portion of the Nansen Basin, a situation apparently caused by freshwater advected by prevailing winds from the Siberian shelf (Fig. 9). This freshwater was replaced by salty intermediate water that upwelled along the Laptev and East Siberian slope to the surface. The centre of the maximum, with salinity greater than 34 ppt, was near Severnaya Zemlya.

Thus, Russian observations (Nikiforov & Shpaikher 1980; this study) have shown very strong salinification events in the Nansen Basin in the

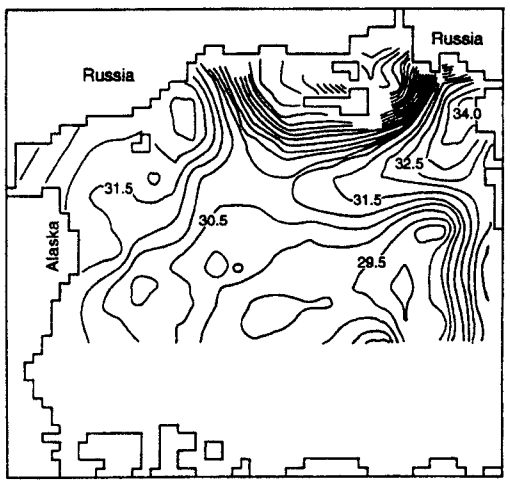

Fig. 9. Winter 1979 surface salinity (ppt). Contour interval is 0.5 ppt.

past, which attest to the conclusion that the salinification in the 1990s (Steele & Boyd 1998) was not unique. The most probable reason for this phenomenon is anomalous winds, as suggested by Nikiforov & Shpaikher (1980) and Steele & Boyd (1998), and not increased warm and salty Atlantic water coming in via the Barents Sea as suggested by Zhang et al. (1998). Our diagnostic computations demonstrate that ocean circulation, as well as salinity, is influenced by such anomalous atmospheric conditions.

Acknowledgements. – We thank the anonymous referees for many useful comments.

References

Aagaard, K.1989: A synthesis of the Arctic circulation. *Rapports et proces-verbaux des reunions / Conseil permanent international pour l'exploration de la mer. 188*, 11–22.

Blumberg, A. F. & Mellor, G. L. 1983: Diagnostic and prognostic numerical circulation studies of the South Atlantic Bight. *J. Geophys. Res. 88*, 4579–4592.

Demin, Yu. L., Friedrich, R. A., Ibraiev, A. S., Sarkisyan, A. S. & Sundermann, J. 1991: A note on modelling the world ocean climate. *Ocean Modelling 89*, 10–11.

Engedahl, H. 1995: Use of the flow relaxation scheme in a three-dimensional baroclinic ocean model with realistic topography. *Tellus. 47A(3)*, 365–382.

Ezer, T. & Mellor, G. L. 1994: Diagnostic and prognostic calculations of the North Atlantic circulation and sea level using a sigma coordinate ocean model. *J. Geophys. Res. 99(C7)*, 14159–14171.

Gorshkov, S. G. 1980: *Atlas Okeanov. Severnij Ledovitij Okean. (Atlas of Ocean; Arctic Ocean.)* 199 pp. Moscow: Military Defense Publishing House.

Gudkovich, Z. M. 1961: Svjaz' mezdu drejfom l'da v Arkticeskom Bassejne i ledovimi uslovijami v Sovetskih Arkticeskih morjah. (Relationship between ice drift in the Arctic Basin and ice conditions in the Soviet Arctic Seas.) *Trudi Okeanologiceskogo Komiteta (Transactions, Oceanographic Committee) 11*, 145–148. Moscow: Academy of Science, USSR.

Häkkinen, S. 1993: An Arctic source for the Great Salinity Anomaly: a simulation of the Arctic ice-ocean system for 1955–1975. *J. Geophys. Res. 98(C9)*, 16397–16410.

Hibler, W. D. III & Bryan, K. 1987: A diagnostic ice-ocean model. *J. Phys. Oceanogr. 7*, 987–1015.

Holland, W. D. & Hirschman, A. 1972: A numerical calculation of the circulation in the North Atlantic Ocean. *J. Phys. Oceanogr. 2*, 336–354.

Nikiforov, Ye. G. & Shpaikher, A. O. 1980: *Zakonomernosti formirovanija krupnomasstabnih kolebanij gidrologiceskogo rezima Severnogo Ledovotogo okeana. (Features of the formation of hydrological regime large-scale variations in the Arctic Ocean.)* 272 pp. Leningrad: Hydrometeoizdat.

Petrov, L. S. 1983: Struktura atmosferi nad arkticeskim okeanom. (Atmospheric structure over the Arctic Ocean.) *Trudi Arkticeskogo i Antarkticeskogo Naucno-Issledovatel'skogo Instituta. (Transactions, Arctic and Antarctic Research Institute.)* 125 pp. Leningrad: HydroMeteoIzdat.

Polyakov, I. V. 1996: Diagnostic calculations of the currents and sea level variations of the Arctic Ocean. *Izvestiya Atmos. and Ocean. Physics 32*, 637–649.

Polyakov, I. V. & Timokhov, L. A. 1994: Mean fields of temperature and salinity of the Arctic Ocean. *Russian Meteorol. Hydrol. 7*, 33–38.

Polyakov, I. V., Kulakov, I. Yu., Kolesov, S. A., Dmitriev, N. Eu., Pritchard, R. S., Driver, D. & Naumov, A. K. 1998: Coupled sea ice – ocean model of the Arctic Ocean. *J. Offshore Mech. Arctic Eng. 120*, 77–84.

Proshutinsky, A. Yu. & Johnson, M. A. 1997: Two circulation regimes of the wind driven Arctic Ocean. *J. Geophys. Res. 102*, 12493–12514.

Sarkisyan, A. S. 1969: On the shortcomings of barotropic models of the oceanic circulation. *Izvestiya Atmos. and Ocean. Physics 5*, 818–836.

Sarkisyan, A. S. 1991: *Modelirovanije dinamiki okeana. (Modelling of ocean dynamics.)* 295 pp. St. Petersburg: HydroMeteoIzdat.

Sarkisyan, A. S. & Demin, Yu. L. 1983: A semidiagnostic method of sea currents calculation. Large-scale oceanographic experiments in the WCRP. *World Climate Research Programme Publication Series 2(1)*, 201–214.

Sarmiento, J. L. & Bryan, K. 1982: An ocean transport model for the North Atlantic. *J. Geophys. Res. 87*, 394–408.

Serreze, M. C., Barry, R. G. & McLaren, A. S. 1989: Seasonal variations in sea ice motion and effects on sea ice concentration in the Canada Basin. *J. Geophys. Res. 94*, 10955–10970.

Song, Y. & Haidvogel, D. 1994: A semi-implicit ocean circulation model using a generalized topography-following coordinate system. *J. Comput. Phys. 115*, 228–244.

Steele, M. & Boyd, T. 1998: Retreat of the cold halocline layer in the Arctic Ocean. *J. Geophys. Res. 103*, 10419–10435.

Thorndike, A. S. & Colony, R. 1982: Sea ice motion in response to geostrophic winds. *J. Geophys. Res. 87*, 5845–5852.

Treshnikov, A. F. 1985: *Atlas Arktiki. (Atlas of the Arctic.)* 204 pp. Moscow: Main Administration of Geodesy and Cartography.

Zhang, J., Rothrock, D. A. & Steele, M. 1998: Warming of the Arctic Ocean by a strengthened Atlantic inflow: model results. *Geophys. Res. Lett. 25(10)*, 1745–1748.